JTTEE5 17:846–852
DOI: 10.1007/s11666-008-9217-x
1059-9630/$19.00 © ASM International

Peer Reviewed

# Toward Highly Sintering-Resistant Nanostructured $ZrO_2$-7wt.%$Y_2O_3$ Coatings for TBC Applications by Employing Differential Sintering

*R.S. Lima and B.R. Marple*

*(Submitted May 1, 2008; in revised form July 16, 2008)*

**There are still concerns in the scientific community about the stability of nanostructured YSZ coatings at high temperatures. Questions have been raised about the possibility of accelerated sintering of these ultrafine materials and the associated changes in properties that could accompany this sintering. In this work, nanostructured YSZ coatings were engineered to counteract sintering effects by tailoring the coatings to exhibit a bimodal microstructure formed by (i) a matrix of dense YSZ zones (produced from molten YSZ particles) and (ii) large porous nanostructured YSZ zones (produced from semimolten nanostructured YSZ particles) that were embedded in the coating microstructure during thermal spraying. These coatings were subjected to heat treatment in air at 1400 °C for 1, 5, and 20 h. The superior driving force for sintering exhibited by the porous nanozones, when compared to that of the dense zones, caused the nanozones to shrink at much faster rates than those exhibited by the denser matrix zones (i.e., differential sintering), thereby creating a significant network of voids in the coating microstructure. Due to these effects, after 20 h exposure at 1400 °C, the thermal conductivity and elastic modulus values of the conventional coatings were approximately two times higher than those of the nanostructured ones.**

**Keywords** differential sintering, elastic modulus, nanostructured $ZrO_2$-7wt.%$Y_2O_3$ (YSZ), thermal barrier coatings (TBCs), thermal conductivity

## 1. Introduction

### 1.1 Nanostructured YSZ Coatings

There is an ongoing need to develop materials and strategies to enhance the performance of thermal barrier coatings (TBCs). Different approaches have been employed to achieve this goal. One of the possible approaches is based on the thermal spraying of porous nanostructured agglomerated $ZrO_2$-7-8wt.%$Y_2O_3$ (YSZ) powders, in which individual nanostructured YSZ particles are agglomerated via spray-drying into microscopic clusters.

By using this type of feedstock, it is possible to engineer coatings that exhibit a bimodal microstructure, which is formed by particles that were (i) fully molten and (ii) semimolten in the spray jet (Ref 1, 2). The particles that were fully or almost fully molten in the spray jet will form the matrix that will hold the semimolten particles in the coating microstructure (Ref 1, 2). The semimolten agglomerates, if embedded in porous form in the coating microstructure (i.e., without the complete infiltration of molten material into the capillary network of each agglomerate), will provide the coating a distinct bimodal behavior concerning its elasto-plastic response (Ref 1).

The preliminary high temperature evaluations of this type of nanostructured YSZ coating (produced from agglomerated powders) have been promising. Liang and Ding (Ref 3) evaluated the thermal shock resistance of nano and conventional YSZ coatings deposited via air plasma spray (APS). The coatings were heated at different temperatures up to 1300 °C for 30 min, followed by subsequent quenching in cool water for 10 min. In the temperature range of 1000 to 1300 °C, the number of cycles to failure of the nanostructured coatings was approximately 2-3 times higher than those of the conventional ones. Wang et al. (Ref 4) heated nanostructured and conventional YSZ APS coatings at 1200 °C for 5 min in a furnace. The coatings were quenched in water (room temperature). The number of cycles to failure of the

This article is an invited paper selected from presentations at the 2008 International Thermal Spray Conference and has been expanded from the original presentation. It is simultaneously published in *Thermal Spray Crossing Borders, Proceedings of the 2008 International Thermal Spray Conference*, Maastricht, The Netherlands, June 2-4, 2008, Basil R. Marple, Margaret M. Hyland, Yuk-Chiu Lau, Chang-Jiu Li, Rogerio S. Lima, and Ghislain Montavon, Ed., ASM International, Materials Park, OH, 2008.

**R.S. Lima** and **B.R. Marple**, National Research Council of Canada, 75 de Mortagne Blvd., Boucherville J4B 6Y4, QC, Canada. Contact e-mail: rogerio.lima@cnrc-nrc.gc.ca.

nanostructured coatings was 2-4 times higher than those of the conventional ones.

### 1.2 Differential Sintering and Nanomaterials

Despite these interesting preliminary results, there are still open questions concerning the stability of these coatings at high temperatures. Based on sintering principles, it is frequently hypothesized that these nanostructured YSZ coatings will exhibit excessive sintering rates at temperatures above 1200 °C, thereby impeding the application of these coatings as TBCs due to significant increases of thermal conductivity and elastic modulus (stiffness) values, which will lead to premature coating failure.

However, previous work has shown that the application of the concept of differential sintering may be an important strategy to counteract sintering effects in TBCs (Ref 5). This concept is based on the differential sintering rates exhibited by coatings that possess bimodal microstructures engineered from porous nanostructured agglomerated powders, and will be explained in more detail in the following sections. The present work aims at further investigating these effects by determining with a higher degree of precision the thermal conductivity and elastic modulus ($E$) values of nanostructured and conventional YSZ APS coatings subjected to heat treatment in air at 1400 °C for 1, 5, and 20 h.

## 2. Experimental Procedure

### 2.1 Thermal Spraying and Feedstock Powders

Two powders, one nanostructured and one conventional YSZ ($ZrO_2$-7-8wt.%$Y_2O_3$), were employed in this study. The nanostructured YSZ (Nanox S4007, Inframat Corp., Farmington, CT) was sprayed using an $Ar/H_2$ APS torch (F4-MB, Sulzer-Metco, Westbury, NY). The conventional YSZ (Metco 204B-NS, Sulzer-Metco, Westbury, NY) was also sprayed using an $Ar/H_2$ APS torch (9MB (GH nozzle), Sulzer-Metco, Westbury, NY). The particle size distribution of both powders was evaluated by a laser diffraction particle analyzer (Beckman Coulter LS 13320, Beckman Coulter, Miami, FL). The as-received nanostructured powder exhibited a powder size distribution varying from approximately 10 to 150 μm. Sieving was employed to remove smaller particles from this initial size distribution to produce a distribution containing coarser particles. The as-received nanostructured powder was sieved using a 53 μm (Mesh 270) USA Standard Testing Sieve in order to try to obtain a particle size distribution range of ~50 to 150 μm.

The conventional powder was sprayed based on the standard spray conditions recommended by the manufacturer of the powder and torch (i.e., Sulzer-Metco). The spray parameters employed to deposit the nanostructured coating were developed internally. Before coating deposition, the temperature and velocity of the sprayed particles were measured via a diagnostic tool (Accuraspray, Tecnar Automation, Saint-Bruno, QC, Canada). The particle detector was placed at the same spray distance as used to deposit the coatings, i.e., 10 and 11 cm from the torch nozzle for the nanostructured and conventional powders, respectively. Both powders were sprayed on low-carbon steel substrates. The maximum coating surface temperature for all depositions was approximately 160 °C (measured via a pyrometer). Coating thickness was approximately 450-500 μm. The powder feed rate (for both powders) used for coating deposition was 30 g/min.

### 2.2 Heat Treatment

Before heat treatment the low-carbon steel substrates were dissolved in an acidic liquid to produce freestanding YSZ coatings. The heat treatment was carried out in a furnace (in air) at 1400 °C for periods of 1, 5, and 20 h. The furnace reached the plateau of 1400 °C after a dwell time of 60-90 min. After the heat treatment, the samples were removed from the furnace and allowed to cool at room temperature, which was reached after approximately 30 min.

### 2.3 Microstructural Evaluation

The structural characteristics of powders and coatings were evaluated using a field-emission scanning electron microscope (FE-SEM) (S-4700, Hitachi Ltd., Tokyo, Japan). During the metallographic preparation, to better preserve and reveal the true structural features of the coatings, the following procedure was carried out. The coatings were first vacuum impregnated and mounted in epoxy resin, then cut using a diamond saw. Subsequently, the pre-impregnated coatings were remounted in epoxy resin using again vacuum impregnation and polished using standard metallographic procedures.

### 2.4 Mercury Intrusion Porosimetry

The mercury intrusion porosimetry (MIP) technique was used to determine the density and porosity distribution of the as-sprayed and heat-treated freestanding coatings. The MIP evaluation was carried out by a private laboratory (Poremaster 60, Quantachrome Instruments, Boynton Beach, FL). Just one sample per coating was evaluated.

### 2.5 Thermal Conductivity

The thermal conductivity value ($k$) (W/mK) can be calculated by the following equation: $k = \alpha \times C_p \times \rho$; where $\alpha$, $C_p$, and $\rho$ are, respectively, the thermal diffusivity ($m^2/s$), heat capacity ($J/kg \cdot K$), and density ($kg/m^3$) values of the coating. The thermal diffusivity values were obtained via the laser-flash method. The experimental conditions in which these values were obtained are described in more detail in a previous reference (Ref 5). One sample per coating was evaluated. The density values of the coatings were obtained via MIP. The value of heat capacity for the YSZ coatings was taken from the

literature. Antou et al. (Ref 6) measured the heat capacity of a YSZ APS coating continuously from room temperature up to ~550 °C. It was observed that the specific heat of the coating was approximately constant within this temperature range: average value (three samples) of 454 ± 17 J/kg · K.

### 2.6 Elastic Modulus

The $E$ values of as-sprayed and heat-treated free-standing coatings were measured via laser-ultrasonics on the in-plane direction, i.e., parallel to the (original) substrate surface. This measurement is done in the following way. A laser pulse on the coating surface generates an ultrasound wave that propagates and is detected by a second laser located on the same surface but positioned away from the generating source of pulses. The velocity of the acoustic wave on the coating is measured based on the known distance between the source laser and the detection laser, and the time taken from the pulse generation to its detection. The $E$ value (Pa) of a material (coating) can then be calculated by using the following equation: $E = \rho \times v^2$; where $\rho$ and $v$ are, respectively, coating density (kg/m$^3$) (measured via MIP in this work) and laser ultrasound velocity values in the coating (m/s). Just one sample per coating was evaluated; however, each velocity value represents an average of 5 to 10 measurements repeated twice. More details on these measurements can be found in previous work (Ref 5).

## 3. Results and Discussion

### 3.1 Particle Size Distribution

The particle size distributions of the sieved nanostructured and as-received conventional YSZ powders are shown in Fig. 1. It is possible to observe that the nanostructured powder exhibits a particle size distribution significantly larger than those of typical ceramic thermal spray powders, i.e., almost 50% of the particles exhibit diameters larger than 100 μm. As shown in the next sections, this characteristic is paramount for engineering the differential sintering phenomenon.

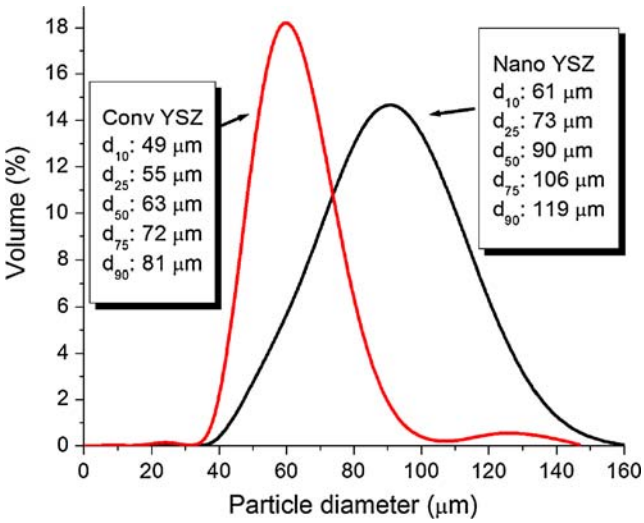


**Fig. 1** Particle size distribution of the conventional and sieved nanostructured YSZ powders

### 3.2 Powder Morphology

The surface characteristics of the nanostructured and conventional YSZ powders can be observed in Fig. 2 and 3, respectively. The nanostructured powder was produced (agglomerated) via spray-drying and sintering of individual nanostructured YSZ particles. It is possible to distinguish the porous and ultrafine characters of the agglomerates.

The conventional YSZ powder was produced via spray-drying and subsequently plasma spheroidization to form hollow spherical particles. Due to this process, the

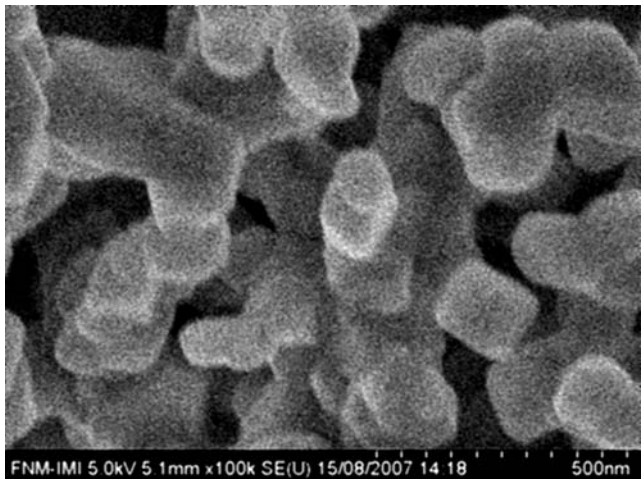


**Fig. 2** Surface of the nanostructured YSZ powder


**Fig. 3** Surface of the conventional YSZ powder

individual spray-dried particles were almost completely molten, and without any significant ultrafine character (Fig. 3).

### 3.3 In-flight Particle Characteristics

The average particle temperatures for the nanostructured and conventional YSZ powders were 2670 °C and 2700 °C, respectively. It is important to point out that the melting point of $ZrO_2$-7-8wt.%$Y_2O_3$ is ~2700 °C (Ref 7). Therefore, it is expected that the YSZ powders arriving at the substrate were composed of fully molten, semimolten, and even nonmolten particles. This is particularly true for the nanostructured feedstock due to its larger overall diameter (Fig. 1). This is an important characteristic to preserve and embed part of the original porous ultrafine structure of the feedstock (Fig. 2) in the coating microstructure. The average particle velocities for the nanostructured and conventional YSZ powders were 210 m/s and 148 m/s, respectively.

### 3.4 As-sprayed Coatings: Microstructure

The microstructure of the conventional YSZ coating is shown in Fig. 4. It exhibits the typical lamellar characteristics and pore structure of YSZ coatings deposited by APS for TBC purposes. The microstructure of the nanostructured YSZ coating contains distinct features (Fig. 5). It is possible to observe a bimodal microstructure, consisting of lighter-colored (dense) and darker-colored regions (Fig. 5a). When the darker zones of the microstructure are observed at higher magnifications, it is possible to distinguish a porous ultrafine structure (Fig. 5b) similar to that of the nanostructured feedstock (Fig. 2). Therefore, these regions represent the semimolten porous nanostructured agglomerated particles that were embedded in the coating microstructure (i.e., the porous nanozones) during thermal spraying. The lighter (dense) zones of Fig. 5(a) represent the previously fully molten nanostructured YSZ particles that form the matrix of the coating microstructure. The percentage of porous nanozones (in cross-sectional area) embedded in the coating microstructure was estimated to be ~35%. A total of 10 SEM pictures were taken (at 500×) and the nanozones were manually selected via image analysis to perform this evaluation. As shown in the next sections, these porous nanozones have a fundamental role during the process of differential sintering.

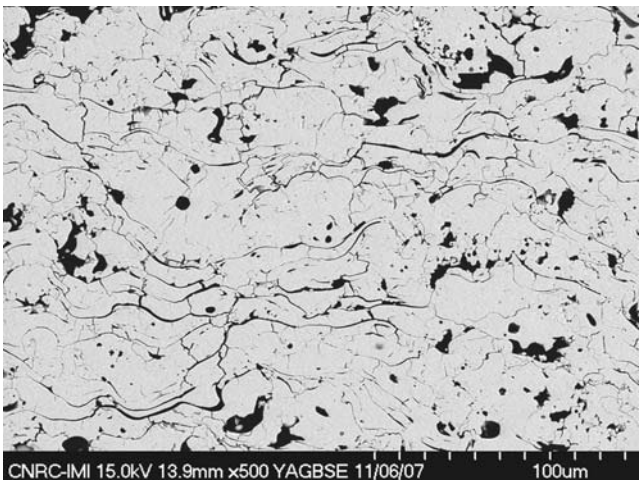


**Fig. 4** As-sprayed conventional YSZ coating

### 3.5 Heat-treated Coatings: Microstructure

The microstructures of the heat-treated nanostructured YSZ coatings are shown in Fig. 6. It is possible to observe that the size and percentage in the cross-sectional area of coarse pores/voids (dark zones) tended to increase with increasing heat treatment time. By comparing the microstructural evolution of these coatings with the microstructural characteristics of the as-sprayed one (Fig. 5), it is somewhat evident that the opening of the coarse pores and voids occurred in the porous nanozones at the interface with the denser matrix regions.

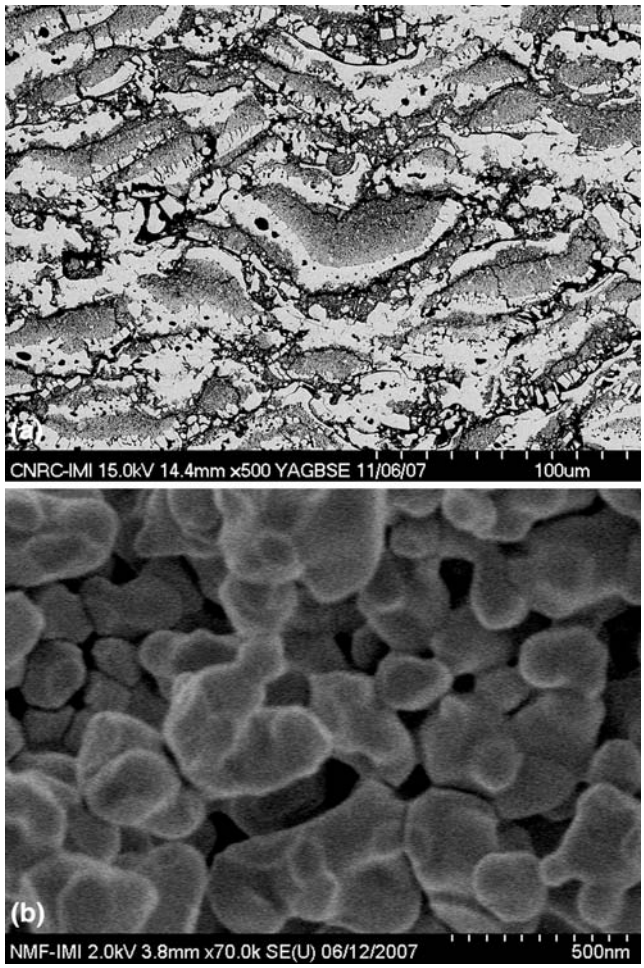


**Fig. 5** As-sprayed nanostructured YSZ coating observed at low (a) and high magnifications (b)

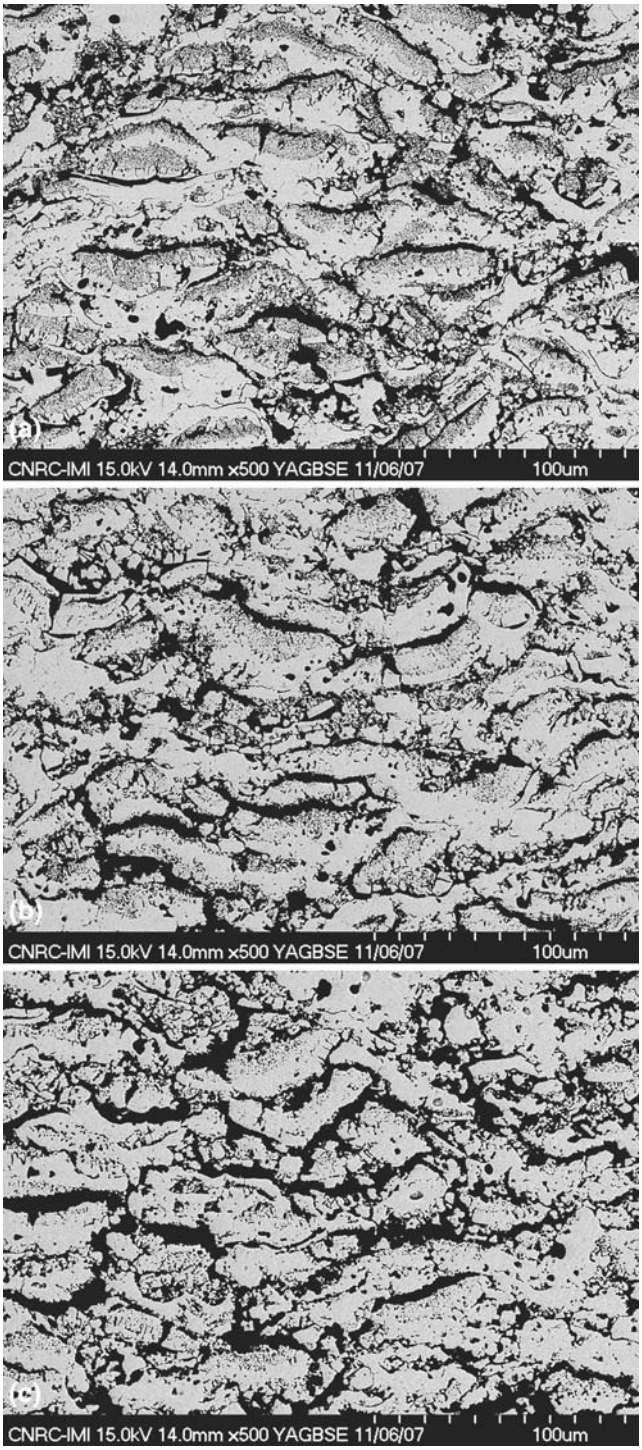


**Fig. 6** Heat-treated (1400 °C) nanostructured YSZ coatings: (a) 1 h, (b) 5 h, and (c) 20 h

The porous nanozones exhibit a much higher driving force for sintering (higher surface area) than that of the dense matrix, which was formed by the particles that were fully or almost fully molten in the spray jet. The difference in the driving force for sintering between the two zones gives rise to a differential sintering effect.

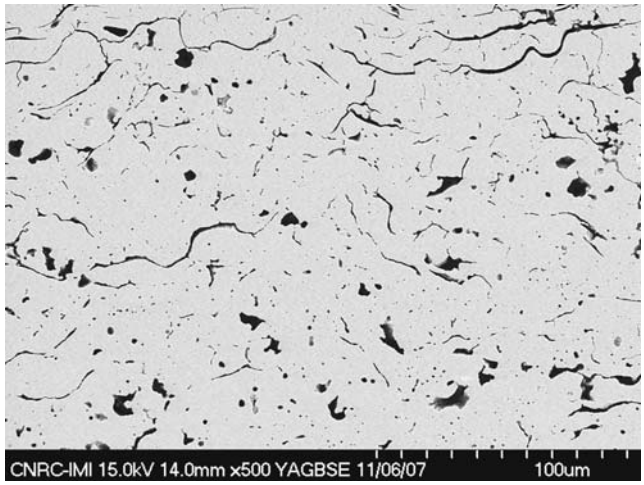


**Fig. 7** Heat-treated (1400 °C/20 h) conventional YSZ coating

The conventional YSZ coating exhibited the typical behavior of a ceramic material exposed at high temperatures for long periods, i.e., the size of coarse pores and voids decreased with heat treatment time. This characteristic can be observed when comparing the microstructures of the as-sprayed (Fig. 4) and heat-treated (1400 °C/20 h) (Fig. 7) conventional coatings.

The porosity values for the as-sprayed and heat-treated YSZ coatings exhibited a range of 11 to 16% for the conventional coatings and 28 to 32% for the nanostructured ones, respectively. This difference in the sintering behavior between nanostructured and conventional YSZ coatings will have a significant impact on the evolution of the elastic and thermal conductivity properties at high temperatures, as depicted in the next sections.

### 3.6 Evolution of Thermal Conductivity

The evolution of thermal conductivity values caused by high temperature exposure for nanostructured and conventional YSZ coatings is shown in Fig. 8. The thermal conductivity value of the as-sprayed conventional coating is almost twice that of the as-sprayed nanostructured coating. Moreover, this difference remains after high temperature exposure. After 1 h exposure at 1400 °C, the thermal conductivity values of both coatings increased substantially.

However, after this point up to 20 h of heat exposure, the thermal conductivity growth rate of the conventional coating [~0.024 (W/mK)/h] is almost five times higher than that of the nanostructured coating [~0.005 (W/mK)/h]. After the 20 h exposure, the thermal conductivity value of the conventional coating is two times higher than that of the nanostructured one. It has to be pointed out that Zhu and Miller (Ref 8) reported a thermal conductivity value of ~1.45 W/mK for a conventional APS YSZ coating after an exposure of 20 h at 1320 °C, i.e., within the range found in this study for the conventional coating after a 20 h exposure at 1400 °C (Fig. 8). In fact, the thermal conductivity value of the nanostructured coating after 20 h

of heat treatment (~0.9 W/mK) is within the range of values generally reported for as-sprayed conventional YSZ coatings, i.e., ~1 W/mK (Ref 8).

### 3.7 Evolution of Elastic Modulus

The evolution of $E$ values caused by high temperature exposure for nanostructured and conventional YSZ coatings is shown in Fig. 9. The $E$ value of the as-sprayed conventional coating is about eight times higher than that of the as-sprayed nanostructured one. After 1 h of heat treatment, the $E$ values of both coatings increase significantly; however, for longer heat treatment times the $E$ values of the conventional coating continue to increase almost linearly at a rate of ~2.4 GPa/h, whereas the $E$ values of the nanostructured coating exhibit a much smaller rate of increase of ~0.5 GPa/h. After a 20 h exposure at 1400 °C, the $E$ value of the conventional coating is about twice that of the nanostructured one.

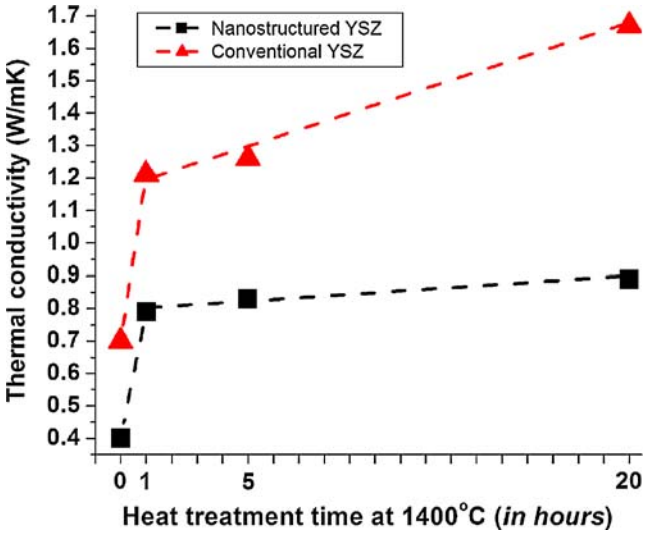


**Fig. 8** Evolution of thermal conductivity values from as-sprayed to heat-treated coatings

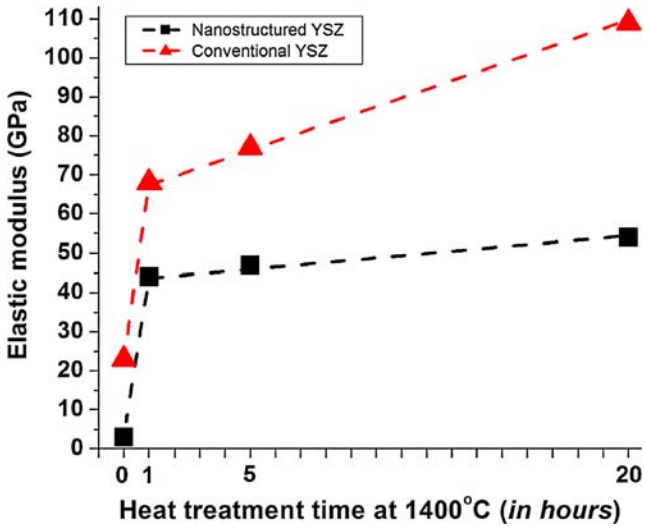


**Fig. 9** Evolution of elastic modulus values from as-sprayed to heat-treated coatings

### 3.8 Role of Differential Sintering

The process of differential sintering has a major role in the evolution of thermal conductivity and elastic modulus values of the YSZ coatings observed in this study. Concerning the nanostructured coating, porous nanostructured agglomerates (nanozones) embedded in the coating microstructure (Fig. 5) during thermal spraying exhibited much higher sintering rates than those of the fully molten ones, which formed the dense matrix of the system. The driving force for this higher sintering rate was strongly associated with the higher surface area provided by the nonmolten and noninfiltrated YSZ nanoparticles. At high temperature exposure, these porous nanozones shrank much faster than the matrix, which led to the opening of large micron-sized voids in the coating structure (Fig. 6). It is important to point out that both coatings exhibit an overall densification of their microstructures. The density values of the conventional coating increased from 4.35 g/cm$^3$ (as-sprayed) to 4.79 g/cm$^3$ (1400 °C/20 h), whereas those of the nanostructured coating increased from 3.92 g/cm$^3$ (as-sprayed) to 4.05 g/cm$^3$ (1400 °C/20 h). However, the opening of the coarse micron-sized voids in the nanostructured coating as shown in Fig. 5 and 6, counteracted sintering effects on thermal conductivity and stiffness, as observed in Fig. 8 and 9. MIP analysis confirms this trend (Fig. 10). The overall size of the pores of the nanostructured coating increased after the heat treatment, whereas the overall size of the pores of the conventional coating decreased after heat treatment (Fig. 10), as also observed in Fig. 4 and 7, i.e., the typical behavior of conventional materials.

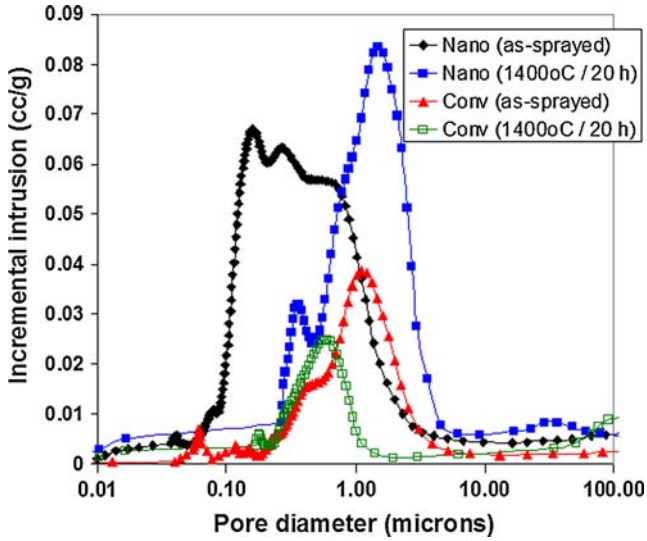


**Fig. 10** Evolution of pore diameter values measured via MIP from as-sprayed to heat-treated coatings at 1400 °C/20 h

It is important to point out that Racek et al. (Ref 9) also observed void opening caused by heat treatment due to the shrinkage of porous nanozones in nanostructured YSZ thermal spray coatings. However, in that study the evolution of thermal conductivity and elastic properties with temperature were not investigated.

### 3.9 Final Comments

Kulkarni et al. (Ref 10) carried out a detailed comparison about the effect of the morphology of YSZ powders on the microstructure, thermal conductivity, and elastic modulus values of APS YSZ coatings. Four powder morphologies were employed: fused and crushed (F&C), sol gel manufactured (SG), spray-dried and sintered (SD), and hollow sphere (HS).

The YSZ coatings produced from the HS powder exhibited the lowest values of thermal conductivity and elastic modulus of all coatings produced, even though they were not the most porous coatings. In fact, the SD coating was the most porous of the four types of coatings, but due to a series of microstructural factors, this higher porosity did not translate into lower thermal conductivity and elastic modulus values.

In another paper of Kulkarni et al. (Ref 11), conventional APS YSZ coatings produced from SD and HS powders were heated-up to 1400 °C (the same temperature used in this study) and their thermal conductivity values were measured. The same trend was observed, i.e., the thermal conductivity values of the HS coatings were lower than those of the SD coatings after high temperature exposure.

Therefore, based on thermal conductivity and elastic modulus values, it seems to be logical to choose HS YSZ coatings (the best performing material) to be compared to these nanostructured YSZ coatings. In addition, the HS YSZ powders are among the most employed powders today for the production of YSZ coatings for TBC applications. Therefore, it is the current benchmark of the turbine industry. It is for these reasons that the conventional YSZ powder employed in this work is also a HS type.

It has to be stressed that the microstructures of the conventional YSZ coating (Fig. 4) of this study exhibited the traditional lamellar structure regularly observed for ceramic thermal spray coatings, whereas that of the nanostructured YSZ coating is a novel microstructure (Fig. 5). To carry out this comparison of microstructures was one of the main objective of the authors.

Finally, it is recognized that it would have been interesting to include a micro-SD YSZ powder with similar particle size distribution to that of the nanostructured YSZ powder (i.e., ~50-150 μm) (Fig. 1) in this study. It could help in improving the understanding of the nano-effect in the coating properties and high temperature behavior. This is an ongoing work and this type of experiment should be done in the future.

## 4. Conclusions

It is possible to engineer nanostructured YSZ coatings for TBC applications that counteract sintering effects via differential sintering. This effect is achieved by embedding semimolten porous nanostructured YSZ agglomerates in the coating microstructure during thermal spraying under a careful control of particle size distribution and in-flight particle characteristics. These porous nanozones exhibit a higher driving force for sintering when compared to that of the coating matrix due to their larger surface area, thereby shrinking at faster rates and opening voids within the coating microstructure at elevated temperatures. This localized void creation counteracts overall sintering (densification). After a temperature exposure of 1400 °C for 20 h, the thermal conductivity and $E$ values of the conventional YSZ coating are about two times higher than those of the nanostructured material. This result is considered as very promising.

## References


1. R.S. Lima, A. Kucuk, and C.C. Berndt, Bimodal Distribution of Mechanical Properties on Plasma Sprayed Nanostructured Partially Stabilized Zirconia, *Mater. Sci. Eng. A*, 2002, **327**, p 224-232
2. R.S. Lima and B.R. Marple, Thermal Spray Coatings Engineered from Nanostructured Ceramic Agglomerated Powders for Structural, Thermal Barrier and Biomedical Applications: A Review, *J. Therm. Spray Technol.*, 2007, **16**(1), p 40-63
3. B. Liang and C. Ding, Thermal Shock Resistances of Nanostructured and Conventional Zirconia Coatings Deposited by Atmospheric Plasma Spraying, *Surf. Coat. Technol.*, 2005, **197**, p 185-192
4. W.Q. Wang, C.K. Sha, D.Q. Sun, and X.Y. Gu, Microstructural Feature, Thermal Shock Resistance and Isothermal Oxidation Resistance of Nanostructured Zirconia Coating, *Mater. Sci. Eng. A*, 2006, **424**, p 1-5
5. R.S. Lima and B.R. Marple, Nanostructured YSZ Thermal Barrier Coatings Engineered to Counteract Sintering Effects, *Mater. Sci. Eng. A*, 2008, **485**, p 182-193
6. G. Antou, F. Hlawka, A. Cornet, C. Becker, D. Ruch, and A. Richie, In Situ Laser Remelted Thermal Barrier Coatings: Thermophysical Properties, *Surf. Coat. Technol.*, 2006, **200**, p 6062-6072
7. K. Muraleedharan, J. Subrahmanyam, and S.B. Bhaduri, Indentification of t' Phase in $ZrO_2$-7.5wt%$Y_2O_3$ Thermal-Barrier Coatings, *J. Am. Ceram. Soc.*, 1988, **71**(5), p C-226-227
8. D. Zhu and R.A. Miller, Thermal Conductivity and Elastic Modulus Evolution of Thermal Barrier Coatings under High Heat Flux Conditions, *J. Therm. Spray Technol.*, 2000, **9**(2), p 175-180
9. O. Racek, C.C. Berndt, D.N. Guru, and J. Heberlein, Nanostructured and Conventional YSZ Coatings Deposited Using APS and TTPR Techniques, *Surf. Coat. Technol.*, 2006, **201**, p 338-346
10. A. Kulkarni, Z. Wang, T. Nakamura, S. Sampath, A. Goland, H. Herman, J. Allen, J. Ilavsky, G. Long, J. Frahm, and R.W. Steinbrech, Comprehensive Microstructural Characterization and Predictive Property Modeling of Plasma-Sprayed Zirconia Coatings, *Acta Mater.*, 2003, **51**, p 2457-2475
11. A. Kulkarni, A. Vaidya, A. Goland, S. Sampath, and H. Herman, Processing Effects on Porosity-Property Correlations in Plasma Sprayed Yttria-Stabilized Zirconia Coatings, *Mater. Sci. Eng. A*, 2003, **359**, p 100-111